



Synergetic Effect of Discontinuous Carbon Fibers and Graphite Flakes on Thermo-Mechanical Properties of Aluminum Matrix Composites Fabricated by Solid–Liquid Phase Sintering

Nabil Chamroune¹ · Florence Delange² · Nathalie Caillault² · Fabrice Morvan³ · Yongfeng Lu⁴ · Akira Kawasaki⁵ · Jean-François Silvain^{1,4}

Received: 28 February 2019 / Accepted: 7 June 2019 / Published online: 17 July 2019
© The Korean Institute of Metals and Materials 2019

Abstract

Aluminum (Al) matrix composite materials reinforced with graphite flakes (GF) and pitch-based carbon fibers (CF) were fabricated by solid–liquid phase sintering with a small amount of Aluminum–Silicon eutectic alloy (Al–12 wt%Si). The amount of Al–Si is optimized for a carbon content of 50 vol% in order to achieve, in the plane of GF reinforcement, a higher thermal conductivity (TC) and a lower coefficient of thermal expansion (CTE) compared to identical composite material fabricated by conventional powder metallurgy route. Al/(GF + CF) composite materials were characterized by scanning electron microscopy (SEM), energy-dispersive X-ray microscopy and X-ray tomography in order to highlight the distribution of the Al–Si liquid phase and the formation of a carbon network in the aluminum matrix. A small amount of CF allows to control the through-plane CTE without affecting significantly the in-plane TC of the Al–C composites. The (GF + CF) mixture and the solid–liquid phase sintering allow to achieve a TC of 410 W/m K (in-plane direction) and a CTE of $2.4 \times 10^{-6}/\text{K}$ (through-plane direction), which is, for example, applicable for lightweight heat sink material.

Keywords Metal-matrix composites (MMCs) · Discontinuous reinforcement · Powder processing · Thermal properties

1 Introduction

Metal matrix composite materials (MMC) are currently studied and have several promising applications. One of them concerns their use as heat sinks in microelectronic industries where two conditions are required: a thermal conductivity (TC) as high as possible in order to evacuate the

heat generated by the silicon chip and therefore to increase the reliability of the electronic device, and a coefficient of thermal expansion (CTE) close to the CTE of ceramic substrate ($2\text{--}8 \times 10^{-6}/\text{K}$) and the electronic chip ($2\text{--}4 \times 10^{-6}/\text{K}$) [1–4]. Currently copper (Cu) and aluminum (Al) heat sinks are used because of their high TC (400 W/mK for Cu and 220 W/mK for Al). However, the large CTE mismatch with the ceramic substrate (CTE of Cu equal to $17 \times 10^{-6}/\text{K}$ and CTE of Al equal to $24 \times 10^{-6}/\text{K}$) generates thermo-mechanical stresses at the heat sink-ceramic interfaces which can generate cracks inside the solder joint of inside the ceramic substrate and then catastrophic failure of the electronic device.

Compared to the others matrices (copper or silver), aluminum has a lower TC and a higher CTE. However, due to his low density, and low price, Al has a high specific thermal conductivity (TC divided by density) and low cost which is a great advantage in terms of the fabrication of mobile electronic devices for automobile or aeronautic industries [4].

Among carbon reinforcements, diamonds exhibit outstanding isotropic thermal properties (TC of ~ 2000 W/m K and CTE close to $2.5 \times 10^{-6}/\text{K}$) [5–7]. However, the

✉ Jean-François Silvain
jean-francois.silvain@icmcb.cnrs.fr

¹ CNRS, Univ. Bordeaux, Bordeaux INP, ICMCB, UMR 5026, 33600 Pessac, France

² Schneider Electric SAS, 38TEC, Rue Henry Tarze, 38000 Grenoble, France

³ Toyal Europe SASU, Rte de Lescun, 64490 Accous, France

⁴ Department of Electrical and Computer Engineering, University of Nebraska-Lincoln, Lincoln, NE 68588-0511, USA

⁵ Department of Materials Processing, Graduate School of Engineering, Tohoku University, 6-6-02 Aramaki-aza Aoba, Aoba-ku, Sendai, Miyagi 980-8579, Japan

applications are limited due to its high price and poor machinability. Pitch-based carbon fibers (FC) are in contrast less expensive and have a good machinability but a lower and anisotropic thermal properties (longitudinal direction: TC of 100–1000 W/m K depending on graphitization degree and CTE of $-1 \times 10^{-6}/\text{K}$; transverse direction: TC of 5–10 W/m K and CTE of $12 \times 10^{-6}/\text{K}$) [8, 9]. Graphite flakes (GF) have significant attention for thermal management applications due to their superior thermal properties, low cost and ease of machining. Indeed it has been reported that GF exhibit a CTE of $-1 \times 10^{-6}/\text{K}$ and a TC higher than 1000 W/m K in the plane of graphite flake [10, 11]. A TC of 1600–2000 W/m K has been reported for highly oriented pyrolytic graphite (HOPG) [12, 13]. Out of plane, whatever the graphite type, a TC of 5–10 W/m K and a CTE of $28 \times 10^{-6}/\text{K}$ has been reported [11, 13, 14].

In functional metal matrix composite (MMC), extended works have been reported on reactivity between matrix and reinforcement [15–18], dispersion and orientation of reinforcement [19–21], fabrication process [4] (sintering [10, 21], squeeze casting [10, 22] and pressure infiltration process [23]). However, few attempts in solid–liquid phase sintering [24] have been carried out especially with a mixture of GF and CF reinforcements. Pietro et al. [25] and Oddone et al. [26] reported composites with a mixture of GF and CF, fabricated by gas pressure infiltration and spark plasma sintering, respectively. They focused their studies on sintering parameters (heating rate, current flow and sintering temperature) and the nature of the metal. However, no understanding on the behavior of the thermal properties of Metal/(GF + CF) compared to the Metal/GF and Metal/CF composite materials was reported.

Several studies reported the fabrication of metal/GF composite materials with a significant increase of TC along the GF principal axis (in-plane TC) and a decrease of TC perpendicular to the GF principal axis (through-plane TC) [27, 28]. However, concerning the CTE of MMC, studies reported a slight decrease of the in-plane CTE and, surprisingly, a significant decrease of through-plane CTE [28–31]. In Cu/50 vol%GF systems, through-plane CTE of $2.5 \times 10^{-6}/\text{K}$ [28], $1.9 \times 10^{-6}/\text{K}$ [29] and $-1 \times 10^{-6}/\text{K}$ [30] was reported, which is very close to CTE of silicon ($2.8 \times 10^{-6}/\text{K}$). In Al/50 vol%GF systems, a through-plane CTE of $-10 \times 10^{-6}/\text{K}$ and an in-plane TC of 330 W/m K were reported [31]. However, this CTE presents a significant CTE mismatch with the ceramic substrate. Therefore, in order to obtain a CTE close to $3 \times 10^{-6}/\text{K}$ in Al/GF system, the vol% of GF must be decreased which will, consequently, decrease the TC of Al/GF composite [31].

This investigation reports a way to control the CTE of Al/C composite by adding small quantity of CF to Al/GF composites in order to obtain a CTE compatible to the ceramic in the in-plane or the through-plane direction. Al/

Carbon composites materials were fabricated by solid–liquid phase sintering. The quantity of Al-12 wt%Si alloy, in liquid state during the sintering process, was optimized for a total carbon content of 50 vol% in order to obtain fully dense (Al + Al–Si)/Carbon materials. Different GF/CF ratios was used in order to investigate the effect of the solid–liquid phase sintering and the carbon composition on the TC and the CTE of the (Al + Al–Si)/(GF + CF) composite materials. Al/C composite materials were characterized by scanning electron microscopy (SEM), energy-dispersive X-ray microscopy (EDS) and X-ray tomography in order to understand the behavior of thermo-mechanical properties of Al/(GF + CF) composite materials.

2 Experimental Procedures

2.1 Materials

Gas-atomized Al spherical powder (ULTD0065, Hermillon powders, France, Fig. 1a) and Al-12 wt%Si spherical powder (16-0006G, Toyal, Japan, Fig. 1b) with an average diameter of 10 μm and 8 μm , respectively, were used as the starting metal powder. Graphite Flakes (GF; Yanxin-Graphite Co., Ltd, Fig. 1c), with an average size and thickness of 550 μm and 30 μm respectively, and Carbon Fibers (CF, K223HM, CTN DIALEAD™/BOBBINS, Sumitomo Corporation Europe Limited, Fig. 1d) with an average length and diameter of 250 μm and 10 μm respectively, were added to metal powder. The four components were mixed in Turbula mixer (Turbula Shaker/Mixer Model T2C, Germany) for 2 h to obtain a homogeneous (Al + AlSi)/(GF + FC) distribution.

After compacting the (Al + Al–Si)/C mixture in a steel mold, cylindrical bulk (Al + Al–Si)/C composites ($\text{Ø}10 \times 8 \text{ mm}^3$) were fabricated by hot pressing for 30 min at 600 °C under a uniaxial compressive stress of 60 MPa and primary vacuum. The temperature of the steel mold is measure with a thermocouple place inside the mold and close to the composite powder. Heating time is close to 10 min and cooling time to 60 min. Differential thermal analysis of Al–Si alloy powder has shown that the melting temperature is 578 °C. For these processing conditions, Al–Si alloy is in liquid state during the densification of the materials as illustrated in Fig. 2. The volume fraction of GF and CF in the Al/GF and Al/CF composites respectively, was fixed at 10, 20, 30, 40, and 50%. Concerning Al/(GF + CF) composite materials, the composition of the carbon mixture (vol%GF + vol%CF) was fixed at (48 + 2), (46 + 4), (44 + 6), (42 + 8), (40 + 10), (30 + 20), (20 + 30) and (10 + 40) for a total carbon volume fraction of 50 vol%. The hot-pressing temperature was monitored via a K-type thermocouple located 2 mm from the sample in the steel mold. Considering that the GF and carbon fibers [8, 21] tend

Fig. 1 SEM micrographs of starting materials: **a** Al powder, **b** Al–Si powder, **c** Graphite flakes, **d** Carbon fibers

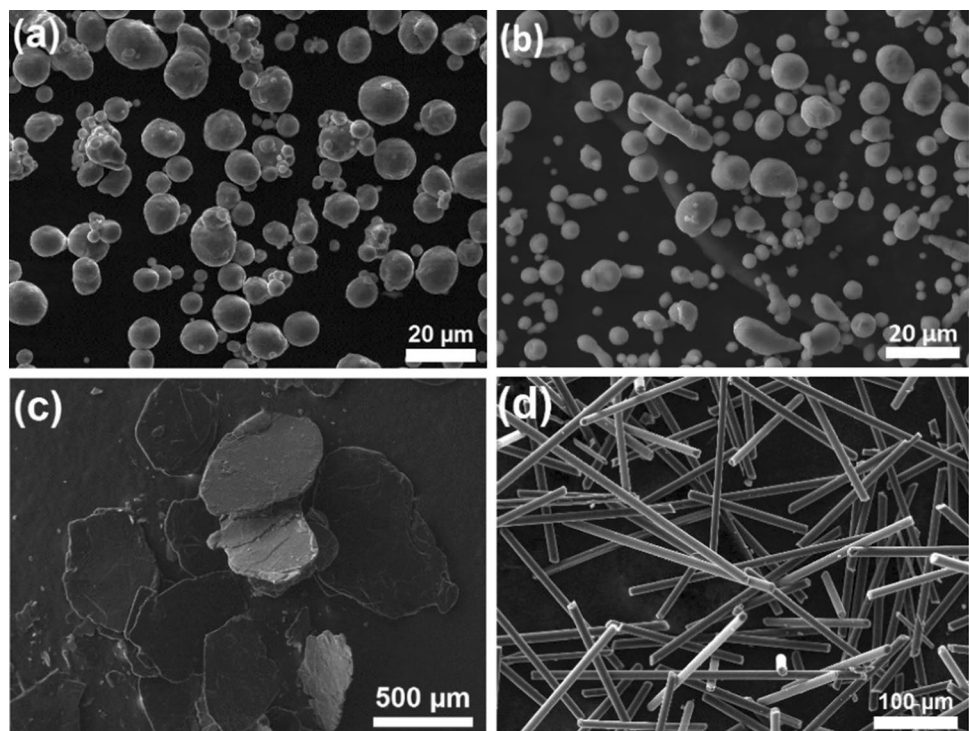
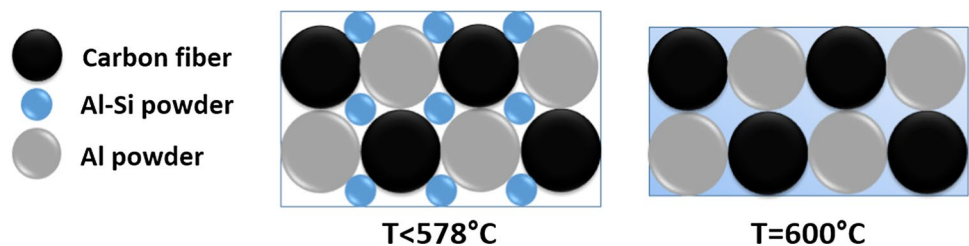


Fig. 2 Illustration of the solid–liquid phase sintering process. The initial powder mixture (Al+ Al–Si + C) is sintered under 60 MPa at 600 °C which result in the fusion of the Al–12 wt%Si alloy



to be aligned perpendicularly to the uniaxial compressive stress, the cylindrical Al/GF composites were machined to $\text{Ø}6 \times 5 \text{ mm}^3$ in order to measure TC and CTE in the in-plane and through-plane direction.

2.2 Characterization

Microstructural characterization of the Al/GF composite was carried out via scanning electron microscopy (SEM, Tescan, VEGA© II SBH). Elemental analysis of the Al/C composites was performed through energy dispersive X-ray spectroscopy (EDS, Apollo X, EDAX Inc.). In order to reveal the microstructure, Al/GF composites were prepared using mechanical polishing with polishing cloth. The polished samples were placed in etchant aqueous solution of sodium hydroxide.

X-Ray tomography was carried out via micro-scanner (General Electrics V/Tome/x s). The acquisition resolution is equal to $2.8 \mu\text{m}^3$. The voltage and rotation resolution are equal to 180 kV and 0.1° , respectively. The dimension of

the sample is $\text{Ø}6 \times 5 \text{ mm}^3$ and $2.5 \text{ mm} \times 2.5 \text{ mm} \times 5 \text{ mm}$. Tomography data were treated with ImageJ software.

The CTE of the Al/C composite materials was measured with a dilatometer (NETZSCH DIL 402, PC) in two thermal cycles from 40 °C to 300 °C with a heating/cooling rates of 2 °C/min, under argon gas flow. The technical mean values of CTE were recorded between 50 °C and 150 °C. Each measure point is an average of 3 samples with a standard deviation close to 3%.

Heat capacity was measured by differential Scanning Calorimetry at 70 °C (DSC 8000 Pyris Diamond PERKIN ELMER) for graphite flake, carbon fiber, Al–Si and Al powders. The TC of Al/GF composites was calculated using the following equation $\text{TC} = \alpha \times \rho \times C_p$ where α is the thermal diffusivity of Al/GF composites measured via the laser flash method (NETZSCH LFA 45, MicroFlash) at 70 °C. Each measure point is an average of 3 samples with a standard deviation close to 5%. The thermal diffusivity was measured in the in-plane and transverse direction. C_p and ρ are the heat capacity and the measured density of the Al/GF composites,

respectively. C_p was calculated from heat capacity of each component by a rule of mixture. Considering that the composite materials only contain closed porosity (ranging from 0.2 to 2.5%), the density of the Al/C composites was measured using the Archimedes principle. The theoretical density of the composites was calculated using a rule of mixture.

3 Results and Discussion

3.1 Microstructure Analysis

Figure 3 shows the in-plane view SEM micrographs of the Al/50 vol%GF (Fig. 3a), Al/vol%(40GF + 10CF) (Fig. 3b), and Al/50 vol%CF (Fig. 3c) composite materials. Dark contrasts are associated to graphite flake (black rectangle) and carbon fiber (black circle) and gray one refers to Al matrix. At that scale of resolution, identical microstructure are found for the Al(Al–Si) matrix. For Al/50 vol%GF and Al/vol%(40GF + 10CF) composites, graphite flakes are preferentially oriented in a plane perpendicular to the pressure direction. In the case of Al/50 vol%(GF + CF), the presence of CF does not affect the orientation of GF compared to Al/GF composite materials. In Al/50 vol%CF composites, carbon fibers are also oriented in the plane perpendicular to the pressure direction but randomly oriented in this plan. Moreover, because of the high-volume fraction of carbon reinforcement (50 vol%), GF–GF (Fig. 4a), GF–CF (Fig. 3b) and CF–CF (Fig. 3c) contact points are observed in all of the Al/C composite materials.

Figure 4 shows X-Ray tomography analysis of Al/50 vol%GF (a, b, and c), Al/vol%(40GF + 10CF) (d, e, f and j) and Al/50 vol%CF (g, h, i, and k) composite materials. The carbon network of Al/50 vol%GF, Al/vol%(40GF + 10CF) and Al/50 vol%CF composites were reconstructed in a cubic block of 1.84 mm^3 . Yellow arrows show the pressure direction (Z axis) applied during the sintering process. These reconstructions clearly show different microstructure observed in (xz) and (xy) plan

which is characteristic of a transversally isotropic material. In the (xy) plan, the top surface of the GF can be observed (Fig. 4c, f, j) whereas the CF are randomly oriented (Fig. 4f, i, k). In the (xz) plan, the section of GF and CF can be observed.

These observations imply that the pressure applied during the hot pressing provides an orientation of the carbon reinforcement perpendicular to the pressure axis. It has to be noticed that in some area, carbon reinforcement is still disoriented [21]. Moreover, the carbon network of Al/vol%(40GF + 10CF), Al/50 vol%CF were reconstructed in a square of $1.1 \text{ mm} \times 1.1 \text{ mm}$ and a thickness of $30 \mu\text{m}$ (Fig. 4j, k).

This allows highlighting the formation of a continuous 2D carbon networks composed by GF and CF oriented randomly in this same plan. However, by comparing Al/vol%(40GF + 10CF) and Al/50 vol%CF, which have the same carbon content, it can be seen an as dense carbon fiber network in Al/vol%(40GF + 10CF) than Al/50 vol%CF. Indeed, in Al/50 vol%CF, the carbon fibers are dispersed in 50 vol% of Al whiles in Al/vol%(40GF + 10CF), the CF are dispersed in lower volume (50 vol% of Al). The dense carbon fiber network observed in Al/vol%(40GF + 10CF) will be used in order to explain further physical properties of the Al/(GF + CF) composite materials.

Figure 5 shows an energy dispersive X-ray spectroscopy (EDS) scan realized on (Al + Al–Si)/50 vol%CF composite material in order to highlight the distribution of the silicon inside the Al matrix. Figure 5b shows the microstructure of Al/CF composites fabricated solid–liquid phase sintering respectively. It shows the presence of white area in the (Al + Al–Si)/50 vol%CF, more precisely in the Al matrix, Al–CF interface and CF–CF contact points. These white parts were not observed in composites fabricated by conventional PM route. The spot 1 and 2 correspond to the aluminum matrix and carbon fiber, respectively. The spots scan 3, 4 and 5 reveals the presence of aluminum and silicon in the white area, which corresponds to the Al–12 wt%Si phase. Then, EDS scan confirms the infiltration of the liquid phase in the

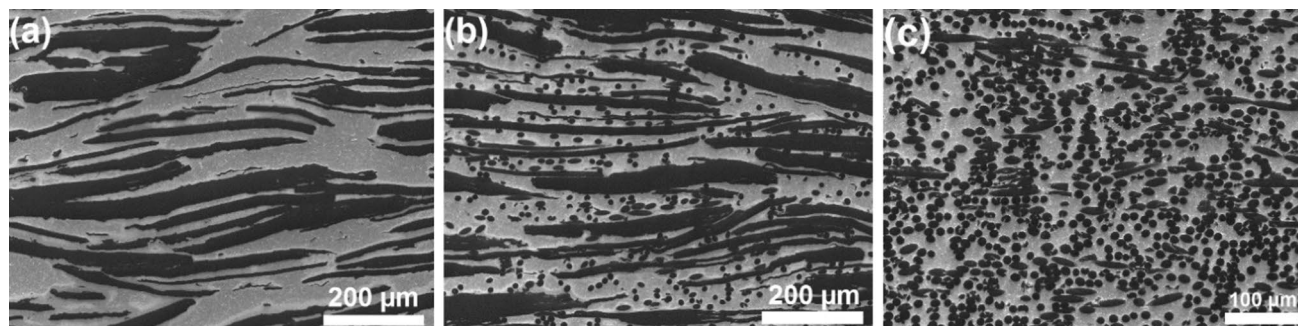


Fig. 3 SEM micrographs (in-plane view) of **a** Al/50 vol% GF, **b** Al/(40 vol% GF + 10 vol% CF) and **c** Al/50 vol%CF composite materials

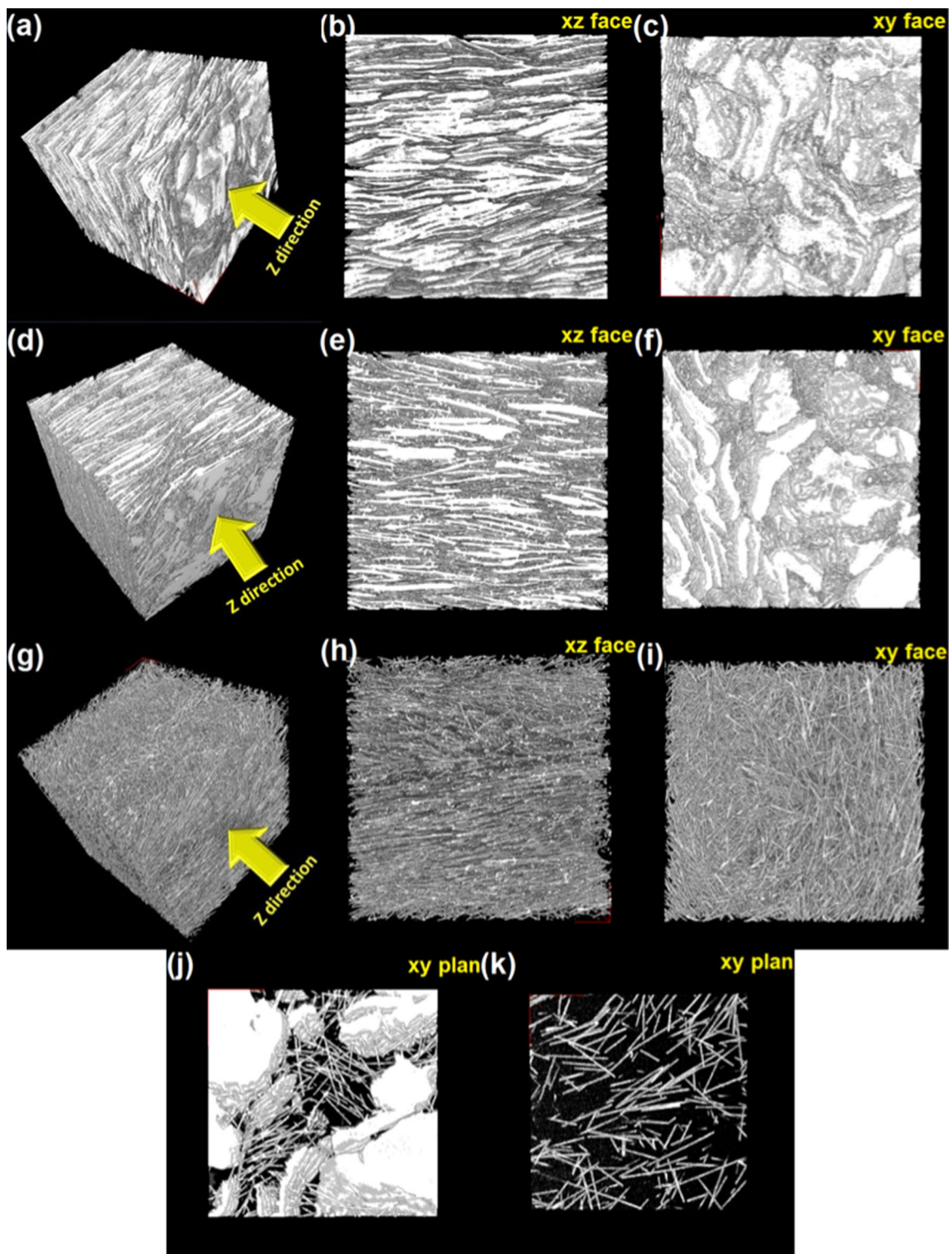


Fig. 4 X-Ray tomography analysis of (a) 3D, (b) 2D (x–z) and (c) 2D (x–y) of the Al/50 vol% GF composite material; (d) 3D, (e) 2D (x–z) and (f–i) 2D(x–y) of the Al/(40 vol% GF + 10 vol% CF) composite

material; (g) 3D, (h) 2D (x–z) and (i–k) 2D (x–y) of the Al/50 vol% CF composite material (Yellow arrows show the pressure direction)

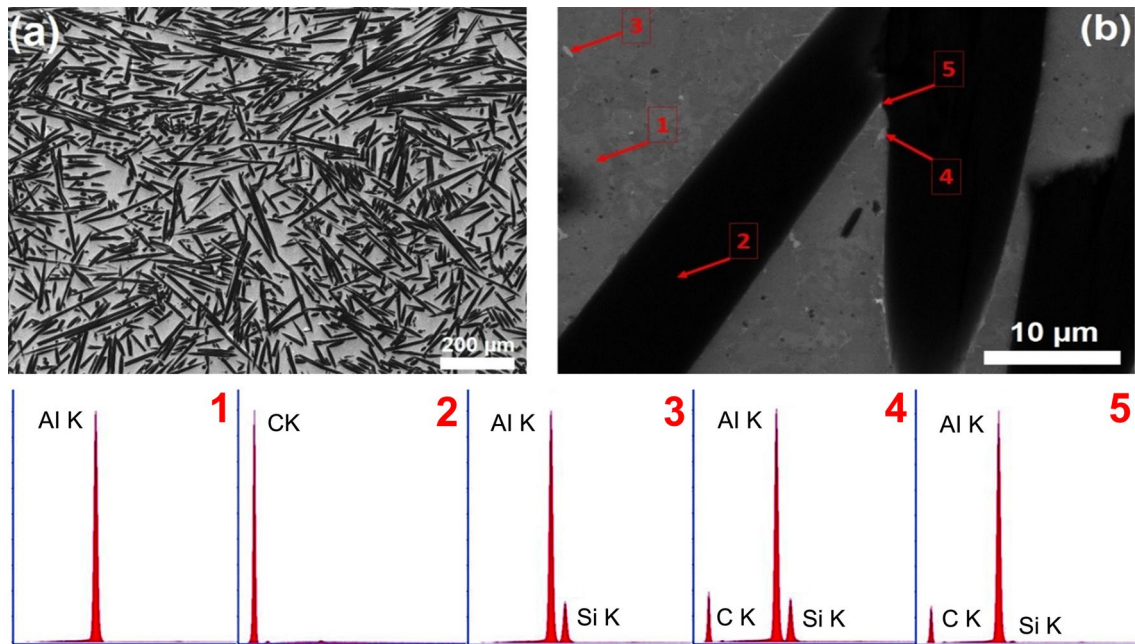


Fig. 5 EDS spot scan analysis of (Al + Al-Si)/50 vol%CF (a, b) composite material

porosity between Al particles, Al-CF interphase and CF-CF contact point during the sintering process.

3.2 Optimization of Solid–Liquid Phase Sintering

The amount of Al-12 wt%Si were optimized for a GF content of 50 vol% in order to achieve a fully dense composite materials and to show its effect on the in-plane TC. Table 1 shows the evolution of the measured relative density of the (Al + Al-Si)/50 vol%GF composite materials with the volume percentage of Al-12wt%Si liquid phase ranging from 0 to 15 vol% with 2.5 vol% step increase. It is well known that the relative density of composites decreases when the reinforcement content increases [16–18, 21]. Indeed, in addition to the porosity, which is inherent to the powder metallurgy (PM) route, the decrease of the relative density may be correlated with the Al-GF interfacial nano-voids [28] and graphite–graphite contact points (Figs. 3, 4) which appear significantly from a carbon volume fraction close to 30 vol%GF [10, 21]. Al/50 vol%GF composite fabricated by conventional PM route shows a relative density of 97.5%. When the volume percentage of liquid phase increases, the relative density increases to reach a value of 98.5% for a

liquid content of 15 vol%. This behavior is explained by the fact that the liquid phase formed during the sintering step, reduces the pores and infiltrates the GF-GF contact point where no sintering can occur. Therefore, the liquid phase sintering helps to increase the relative density of Al/C composite materials with high carbon content. With this fabrication process, MMC, with carbon volume fraction up to 70%, have been successfully fabricated with a porosity level smaller than 3%.

Moreover, Table 1 shows that the evolution of the relative density can be correlated with the evolution of the TC. In the in-plane direction, the graphite flakes are oriented parallel to the direction of thermal conduction measurement. Al/50 vol%GF composite fabricated by conventional PM route shows an in-plane TC of 400 W/m K. From 0 to 5 vol% of liquid phase, the in-plane TC increases from 400 to 425 W/m K. Then, from 5 to 10 vol% of liquid phase, the in-plane TC reaches values close to 425 W/m K, and then decreases at 409 W/m K for higher Al-Si content. It has also to be noticed that, whatever the Al-Si content, the in-plane TC of (Al + Al-Si)/GF composites are always higher than the Al/50 vol%GF fabricated by conventional PM route. This behavior can be explained by two factors: (1)

Table 1 Influence of the Al-12 wt%Si liquid content (vol%) on the relative density (%) and the in-plane TC (W/m K)

Liquid phase content (vol%)	0	2.5	5	7.5	10	12.5	15
Relative density (%)	97.5	97.9	98.1	98.3	98.2	98.3	98.5
In-plane TC (W/m K)	400	404	425	423	428	414	409

the increase of relative density with the liquid phase content and (2) the lower intrinsic TC of Al-12 wt%Si alloy compared to the pure Al (experimental values of 163 W/m K and 217 W/m K, respectively). Indeed, the increase of TC from 0 to 10 vol% of liquid phase is correlated to the increase of the relative density of (Al + Al-Si)/GF composite materials. Then, from 10 to 15 vol% of Al-Si, even if the relative density increases slightly, the important quantity and the intrinsic TC of Al-Si alloy, results in a decrease of the in-plane TC of (Al + Al-Si)/50 vol%GF composite materials. Hence, a volume percentage of 10% were selected in order to fabricate (Al_{90 vol%} + Al-Si_{10 vol%})/50 vol% Carbon composites, where the carbon is a mixture of graphite flakes and carbon fibers.

3.3 Thermal Conductivity of Al/GF and Al/CF Composite Materials

Al/GF and Al/CF composites were fabricated in order to evaluate the individual effect of the GF and CF on the thermal properties of Al/C composite materials. Figure 6 shows the evolution, of the in-plane and through-plane TC of Al/GF and Al/CF composites with different carbon volume fraction. First of all, Fig. 6 shows a TC of 218 W/m K for the sintered Al powder. (TC of 239 W/m K is reported for high purity aluminum at 70 °C [32]). The difference between sintered and high purity aluminum materials (foundry route) is mainly attributed to the residual porosity and the amorphous aluminum oxide presents on the surface of each aluminum grain when using PM route.

In the in-plane direction, the graphite flakes are preferentially oriented parallel to the direction of thermal conduction measurement. Then, the TC increases with the graphite

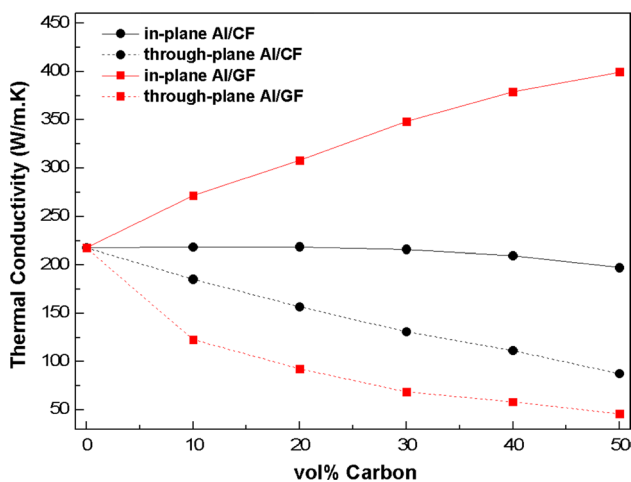


Fig. 6 Comparison of experimental TC of Al/GF (red square) and Al/CF (black circle) composite materials in the through-plane (dotted line) and in-plane (line) direction

content to reach a value of 400 W/m K. This behavior is in accordance to the intrinsic in-plane TC of the GF (close to 1000 W/m K [10, 11]). The TC of the Al/CF composites decreases slightly from 218 to 216 W/m K from 0 to 30 vol% of CF and then reach a value of 197 W/m K from 30 to 50 vol% of CF. This slight decrease of TC may be explained by the fact that, due to the random distribution of the CF in the plane of measurement, the supposed intrinsic TC of the CF in the plane, 280 W/m K [16–18] is an average of the along (550 W/m K; manufacturer data) and perpendicular to the CF axis (5–10 W/m K). Thermal resistance at the Al-C interface and the decrease of the relative density with the increase of carbon content can explain the slight decrease of in-plane TC of Al/CF composite materials.

In the through-plane direction (dotted line), the GF and CF are preferentially oriented perpendicularly to the direction of thermal conduction measurement. Then, the TC decreases with the carbon content to reach a value of 87 and 46 W/m K for Al/GF and Al/CF composites, respectively. This decrease is in accordance to the intrinsic through-plane TC of the GF and CF (5–10 W/m K [10, 11]). However, the behavior of through-plane TC with the carbon content differs between the two reinforcements. Indeed, in the Al/GF composites, the variation of the TC with the GF content has a behavior of an inverse function: a drastic decrease of TC from 0 to 10 vol% of GF (218–123 W/m K: 43% of decrease) and a slower decrease of TC from 10 to 50 vol% of GF (123–46 W/m K: 62% of decrease). In contrast, the TC of Al/CF composites decreases linearly with CF content and stay higher than Al/GF for 50 vol% of carbon. This difference of behavior can be explained by the difference of morphology of the reinforcement. Indeed, the planar morphology and larger size (average size and thickness of 550 μm and 30 μm, respectively) than CF (average length and diameter of 250 μm and 10 μm, respectively) allow the GF to slow the thermal flow more efficiently than CF in the through-plane direction. Moreover, the orientation of the reinforcement, in a plane perpendicular to the pressure direction, which is induced by the hot-pressing process, is easily achieved for the GF than for the CF (Fig. 5a).

3.4 Thermal Conductivity of Al/(GF + CF) and (Al + Al-Si)/(GF + CF) Composite Materials

Figure 7 shows the evolution of the CT of Al/(GF + CF) and (Al_{90 vol%} + Al-Si_{10 vol%})/(GF + CF) composites with a total carbon content of 50 vol%, in the in-plane (Fig. 7a, c) and through-plane (Fig. 7b) directions. For comparison purpose, the CT of Al/GF composite materials was added in Fig. 7a (dotted line). It can be shown that the in-plane TC of the Al/(GF + CF) composites is lower than the Al/GF composites with the same volume content of GF. It should be noted that the gap between the two sets of materials decreases when

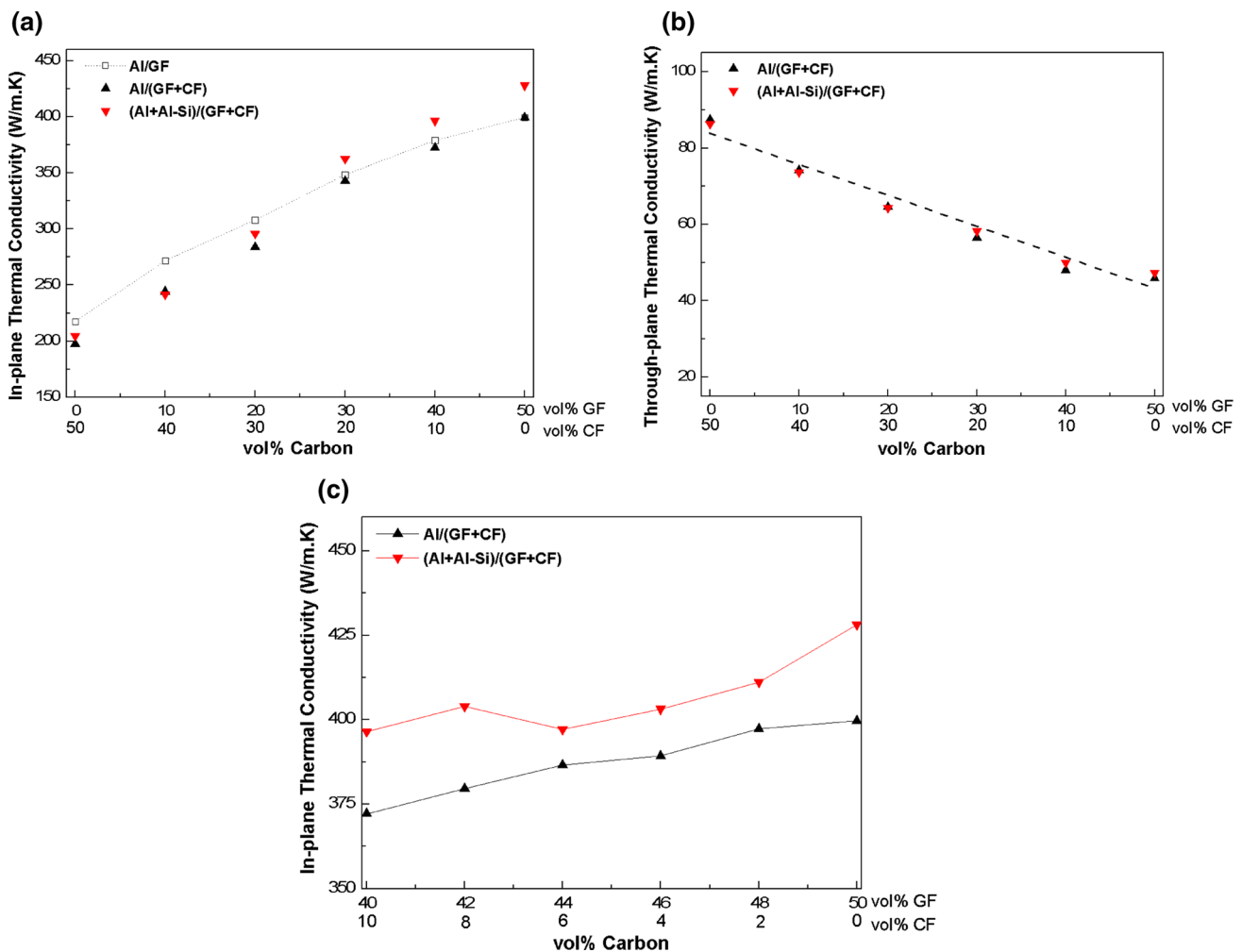


Fig. 7 Experimental CT of $(Al_{90\text{ vol}\%} + Al-Si_{10\text{ vol}\%})/(GF + CF)$ (red triangle) and $Al/(GF + CF)$ (black triangle) composite materials in the in-plane (a and c) and through-plane (b) direction

the GF/CF ratio increases. Indeed, as shown in Fig. 6, the decrease of the in-plane TC of Al/CF is negligible between 0 to 30 vol% of CF which explains the weak gap between $Al/(GF + CF)$ and Al/GF from a carbon content of (30 vol%GF + 20 vol%CF). For higher CF content a decrease of the in-plane TC of $Al/(GF + CF)$, compared to Al/GF with the same GF content, is observed. Figure 7b shows the through-plane TC of $Al/(GF + CF)$ composite materials. It can be seen an almost linear behavior of the TC of $Al/(GF + CF)$ composite materials.

The $Al/(GF + CF)$ composite materials fabricated by conventional PM route (black triangle) were compared to the equivalent composites fabricated by solid-liquid phase sintering (red triangle). It can be seen that solid-liquid phase sintering provides an increase of the in-plane TC (Fig. 7a, c). As explained in Sect. 3.2, the liquid phase sintering tends to increase the relative density of Al/C composite materials

with high carbon content by infiltrating the pores and the carbon-carbon contact points where no sintering can occur.

This increase of the relative density of $Al/50\text{ vol}\%C$ and interfacial chemical reactions provides an enhancement of the in-plane TC. Indeed, as it can be seen on Fig. 8, small voids, located at the $Al-CF(GF)$ interface, can be observed on TEM micrographs of Al/CF (Fig. 8a) whereas no such of voids are observed on $(Al + Al-Si)/CF$ composite materials (Fig. 8b). Also, the $Al-Si$ liquid phase can induce the formation of Aluminum carbide ((Fig. 8b), at the $Al-CF$ interface, inducing a better property transfer between the matrix and the reinforcements.

In the through-plane direction, no significant effect of the solid-liquid process is observed which shows that the through-plane TC were not linked to the relative density like the interfacial thermal resistance, as shown by Ren et al. [28].

Fig. 8 TEM micrographs of **a** Al/CF composite material and **b** Al–Al–Si/CF composite material

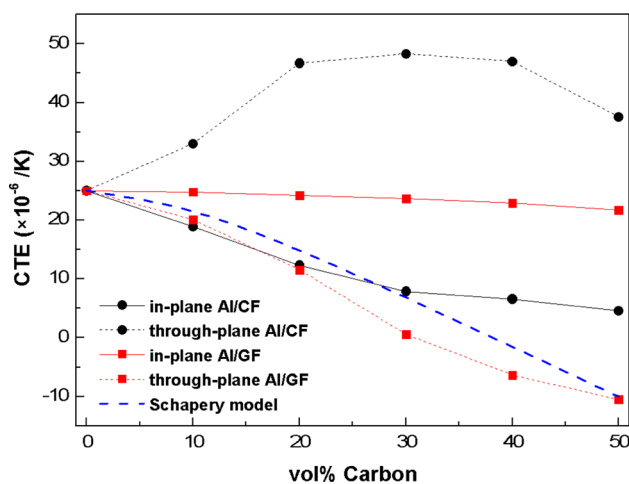
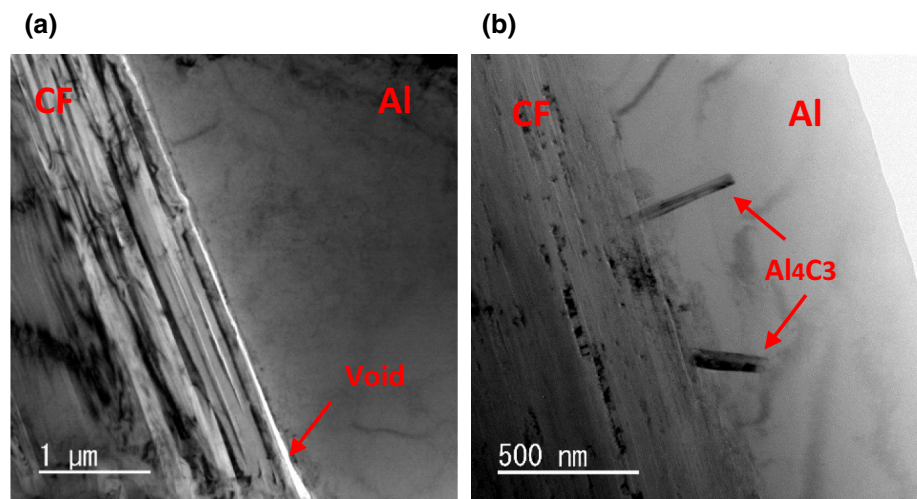


Fig. 9 Comparison of experimental CTE of Al/GF (red square) and Al/CF (black circle) composite materials in the through-plane (dotted line) and in-plane (line) direction. Theoretical predictions by the Schapery model (blue dashed line) for Al/GF system in the through-plane direction

3.5 Thermal Expansion of Al/GF and Al/CF Composites Materials

Figure 9 shows the evolution of the CTE of Al/GF and Al/CF composites with different carbon volume fraction, in the in-plane and through-plane directions. The CTE of pure Al matrix fabricated by PM route has a value of $25 \times 10^{-6}/\text{K}$. Al/GF and Al/CF composites show different behaviors, for the two directions of measurement. Concerning Al/CF composites, a decrease of the in-plane CTE is observed and reaches a value of $4.6 \times 10^{-6}/\text{K}$ for a CF content of 50 vol%. This result is in accordance with the intrinsic in-plane CTE of CF ($-1 \times 10^{-6}/\text{K}$). However, the through-plane CTE of Al/CF composites show an important increase between 0 and 20 vol% of CF, before to reach a maximum value of $47 \times 10^{-6}/\text{K}$ from

20 to 40 vol% and finally, a decrease at 50 vol% CF. Unlike the evolution of the in-plane CTE, this behavior is in contradiction with the intrinsic through-plane CTE of CF ($12\text{--}15 \times 10^{-6}/\text{K}$ [8]). Considering the fact that the CFs restrain the dilatation of Al in the in-plane direction leads to a compressive strain in the same direction and then a decrease of the in-plane CTE [33]. This in-plane compressive strain induces an increase of through-plane CTE because of the positive Poisson ratio of Al and CF (0.345 [27] and 0.2 [34], respectively).

Concerning the Al/GF composites, the CTE differ radically in the two directions of measurement. In the in-plane direction, the CTE decreases slightly to a value of $21.8 \times 10^{-6}/\text{K}$ for 50 vol% of GF. In the through-plane direction, the CTE decreases drastically and reaches a negative value of $-10.5 \times 10^{-6}/\text{K}$ for 50 vol% of GF. These counter-intuitive behaviors were reported in several studies for Al/GF and Cu/GF systems [28–31]. In order to understand these behaviors, Firkowska et al. [29] modeled the mechanical and thermal interplay of graphite and copper within elasticity theory and considered a sandwich-like structure of graphite and copper. They found that the temperature-dependent in-plane strain in the graphite embedded in a matrix copper results in a negative through-plane CTE (α_{33}) of $-26 \times 10^{-6}/\text{K}$ calculated by Eq. (1)

$$\alpha_{33} = \frac{d\varepsilon_{33}}{dT} = \alpha_{gr,3} + \nu_{2D} \Delta\alpha_X - \frac{d\nu_{2D}}{dT} \varepsilon_{11}^0 \quad (1)$$

where ε_{33} and T are the through-plane strain of the graphite and the temperature, respectively. $\alpha_{gr,3}$ is the intrinsic through-plane CTE of graphite ($28 \times 10^{-6}/\text{K}$). ν_{2D} and $\frac{d\nu_{2D}}{dT} = -4.3 \times 10^{-2}/\text{K}$ are the 2D equivalent Poisson ratio of graphite and its temperature derivative. $\varepsilon_{11}^0 \sim -10^{-3}$ is the estimated residual in-plane strain of graphite in copper matrix. $\frac{d\varepsilon_{11}}{dT} = \Delta\alpha_X$ is the temperature derivative of the in-plane strain $\varepsilon_{11} = \varepsilon_{22}$ in graphite and it is calculated using Eq. (2)

$$\frac{d\varepsilon_{11}}{dT} = \Delta\alpha_x = \alpha_x - \alpha_{gr,1} \quad (2)$$

where α_x and $\alpha_{gr,3}$ are the in-plane CTE of Cu/50 vol%GF and GF, respectively. The Eq. (1) shows that the change of CTE value (from $28 \times 10^{-6}/K$ to $-26 \times 10^{-6}/K$) is due to the large Poisson ratio of graphite (ν_{2D}) and its strong temperature dependence.

We propose here to use the formulation (1) of Firkowska et al. [29] to explain the behavior of through-plane CTE of Al/GF composite materials and explain the important decrease of the CTE compared to Cu/GF system. The in-plane lattice constant of the GF follows the CTE of the composites which causes an in-plane strain $\varepsilon_{11} = \varepsilon_{22}$ in the GF that varies with temperature as shown on Eq. (2). In Al/GF system, an in-plane CTE of $21.8 \times 10^{-6}/K$ for 50 vol% of GF was obtained, which is higher than in plane CTE of Cu/50 vol%GF reported in previous studies ($14 \times 10^{-6}/K$ [28], $12 \times 10^{-6}/K$ [29] and $13.6 \times 10^{-6}/K$ [30]). This difference is due to the higher intrinsic CTE of aluminum compared to Copper ($24 \times 10^{-6}/K$ and $17 \times 10^{-6}/K$, respectively [1]). Then the higher in-plane CTE difference of Al/GF and GF ($\alpha_{gr,1} = -1 \times 10^{-6}/K$) induce a higher in-plane strain in the GF. For an Al/GF system $\Delta\alpha_x$ is equal to $22.8 \times 10^{-6}/K$ which is higher than Cu/GF system. In a second step, intrinsic strain, induced by the CTE difference of the different constituent, has to be consider. Indeed, after the consolidation step, when the temperature decreases to room temperature, the reinforcement and the matrix shrink at different rates, which induce a residual in-plane strain ε_{11}^0 equal to $\sim -10^{-3}$ for Cu/GF system [29]. Considering that CTE_{Al} is ~ 1.5 higher than CTE_{Cu} , it can be reasonably assumed that the in-plane residual ε_{11}^0 of Al/GF system is also 1.5 times higher than ε_{11}^0 for Cu/GF system. By using the formulation (1), a value of $-54 \times 10^{-6}/K$ was calculated for the through-plane CTE of GF which is quite different from the intrinsic CTE value of the through-plane GF ($28 \times 10^{-6}/K$). This calculated value will be used to calculate theoretical values of CTE for the Al/GF composite materials.

Schapery model [34] was chosen to predict the CTE of the Al/GF system with anisotropic properties [35] and then compared with the obtained experimental values:

$$\alpha_{c,2} = V_m(1 + \nu_m)\alpha_m + V_f(1 + \nu_{f,2})\alpha_{f,2} - \alpha_{c,1}\nu_{c,1} \quad (3)$$

With

$$\alpha_{c,1} = \frac{V_f\alpha_{f,1}E_{f,1} + V_m\alpha_mE_m}{V_fE_{f,1} + V_mE_m} \quad (4)$$

and

$$\nu_{c,1} = V_m\nu_m + V_f\nu_{f,1} \quad (5)$$

In these equations, α , V , E and ν are the CTE, the volume fraction, the Young's modulus and the Poisson's ratio, respectively. 1 and 2 refer to in-plane and through-plane direction, respectively. The subscripts c, m, and f refer to composite, matrix and reinforcement, respectively. The material parameters for the calculations are given in Table 2 and the through-plane CTE of GF used in this model is the value calculated with the Firkowska formulation [29].

Figure 8 shows a comparison of the theoretical values of the through-plane CTE of Al/GF composite materials (blue dashed line), calculated using Schapery model (3) and Firkowska formulation (1) with the experimental values for fabricated Al/GF composites materials. The Schapery prediction is in fairly good agreement with the experimental CTE of Al/GF composite materials in the through-plane direction. We can therefore argue that the Firkowska formulation, given for Cu based materials, can be transposed for an Al/GF system and allows to demonstrate that the higher mismatch between the matrix and the GF for a Al/GF system compared to a Cu/GF system, induce a higher in-plane strain on the GF and resulting in a through-plane CTE for Al/GF composites significantly lower than for Cu/GF composites.

3.6 Thermal Expansion of Al/(GF + CF) and (Al + Al-Si)/(GF + CF) composite materials

Figure 10 shows the evolution of the CTE of Al/(GF + CF) and (Al_{90 vol%} + Al-Si_{10 vol%})/(GF + CF) composites with a total carbon volume percentage of 50%, in the in-plane (Fig. 10a, c) and through-plane (Fig. 10b, c) directions. For comparison purpose, the CTE of Al/CF and Al/GF composites were added to this figure (dotted line). For pure GF reinforcement, in the in-plane direction, the CTE of the composites decreases slightly to reach value of $21.8 \times 10^{-6}/K$ for 50 vol% of GF. However, with a mix carbon composition (CF + GF), a huge decrease for a CF vol% up to 10% ($9 \times 10^{-6}/K$) is observed (a detail of this variation is given in Fig. 10c) follow by a slower decrease to reach the CTE value of the Al/50 vol%CF material ($4.6 \times 10^{-6}/K$).

Considering that GF alone has no significant effect on the in-plane CTE, Al/(40 vol%GF + 10 vol%CF) can be compared to Al/10 vol%CF composite material. It can be show that for the same content of CF, the CTE decreases from

Table 2 Materials parameters for calculating the theoretical CTE for Al/GF composite materials

Material	α ($10^{-6}/K$)	E (GPa)	ν	References
In-plane GF	-1	1109	0.12	[36]
Through-plane GF	-58 ^a	38.7	0.01	[29] *; [36]
Al	25	69	0.345	[27]

^aValue calculated with Firkowska formulation [29]

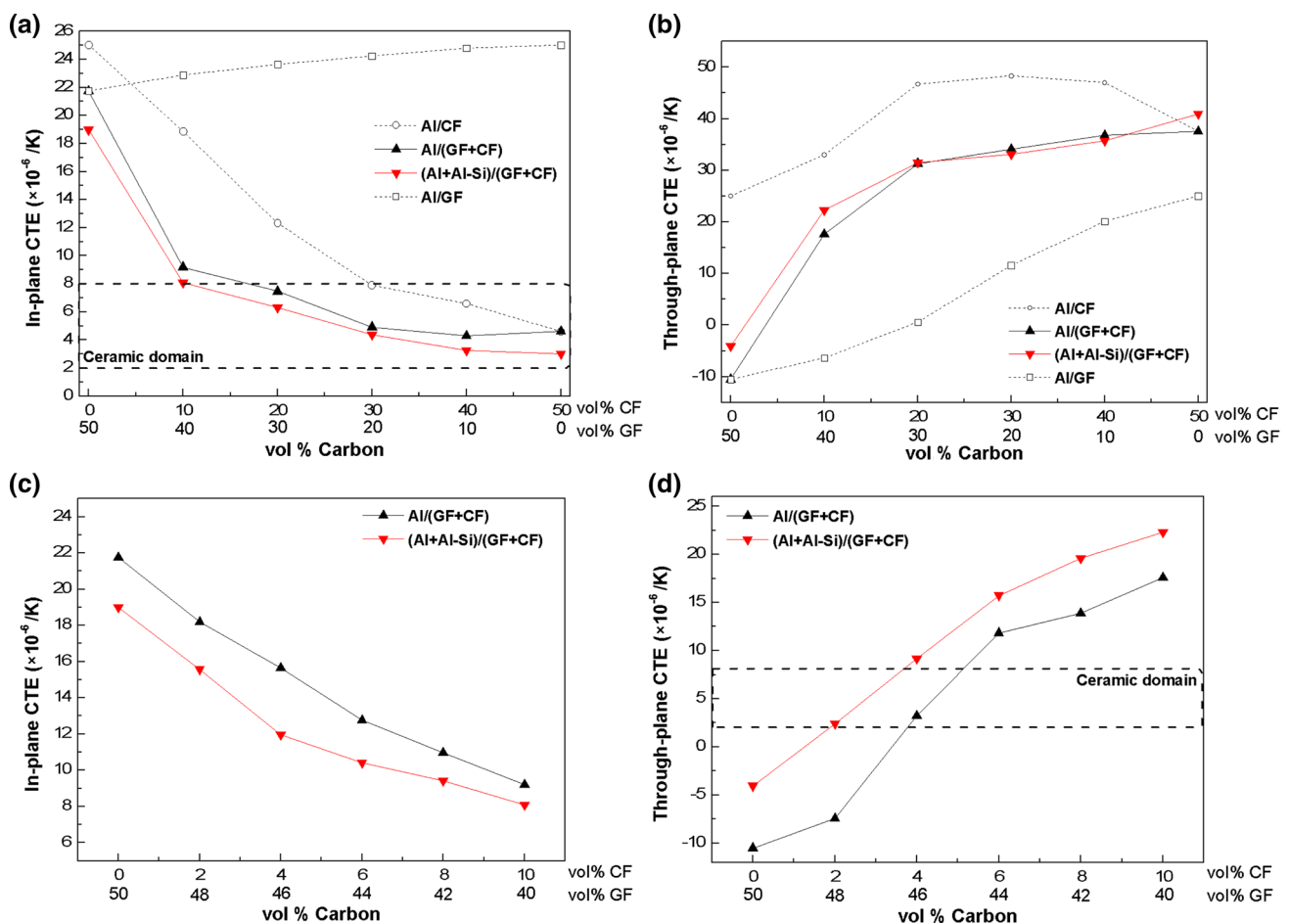


Fig. 10 Experimental CTE of $(Al_{90\text{ vol}\%} + Al-Si_{10\text{ vol}\%})/(GF+CF)$ (red triangle) and $Al/(GF+CF)$ (black triangle) composite materials in the in-plane (a and c) and through-plane (b and c) direction

$18.9 \times 10^{-6}/K$ to $9.2 \times 10^{-6}/K$. Favier et al. [34] reported that the geometric percolation of cylindrical reinforcement, with an aspect ratio of 25, is close to 3 vol% and 18 vol% for a 3D and 2D random orientation, respectively. However, the geometric percolation should be distinguished from the mechanical percolation. Indeed, for electrical system, the geometric percolation is identical with the electric percolation. However, for thermo-mechanical properties, the geometric percolation is not enough to ensure the rigidity of the whole system. Then, the mechanical percolation, which is higher than the geometric percolation, should be considered. The mechanical percolation of the CF in Al/CF composite materials have already been associated to the formation of rigid skeleton of reinforcement, from a CF volume fraction close to 30 vol% [8]. This behavior may explain the slope change of the in-plane CTE observed from 30 vol% of CF (Fig. 10a). The addition of graphite to the CF provides the formation of rigid CF skeleton with only 10 vol% of CF. Indeed, as it was demonstrated by X-Ray tomography, the CF network in $Al/10\text{ vol}\%$ is not enough dense to build a

rigid skeleton, and thus the mechanical percolation is not reached. The huge decrease of CTE for the CF + GF reinforcement can therefore be attributed to the formation of a rigid CF skeleton in-between the network of the graphite flakes. Moreover, the fact that CF are interleaved between GF may prevent the disorientation of CF out of (xy) plane, as observed in $Al/10\text{ vol}\%CF$ composite material (Fig. 4h).

In the through-plane direction, the CTE increases significantly from a value of $-10.5 \times 10^{-6}/K$ for 50 vol% of GF to a value of $37.6 \times 10^{-6}/K$. Indeed, for a carbon composition of (40 vol%GF + 10 vol%CF), an important increase of the CTE is observed and reach a value of $17.6 \times 10^{-6}/K$ (a detail of this variation is given in Fig. 9d). Then, when the CF/GF ratio increases, the CTE increases slowly to tend to the CTE of $Al/50\text{ vol}\%CF$ ($37.8 \times 10^{-6}/K$). Therefore, the addition of CF to the GF provides an important CTE increase of $Al/(GF+CF)$ composite material due to the individual effect of the CF in the through-plane direction showed in Fig. 10b (circle mark and dotted line). The fact that the through-plane CTE decreases in Al/GF composites and increases in Al/CF

composites explains the behavior of Al/(GF + CF) composite materials.

Figure 10 also shows the CTE behavior of the Al based composite materials fabricated using solid–liquid phase sintering (red triangle) where Al–Si eutectic alloy is added to Al. It can be shown that solid–liquid phase sintering provides a decrease of the in-plane CTE and an increase of the through-plane CTE of $(Al_{90 \text{ vol}\%} + Al-Si_{10 \text{ vol}\%})/(GF + CF)$ in comparison to the Al/(GF + CF) composite materials. As shown earlier, the Al–Si liquid phase was observed between the Al particles, at the Al/C interface and at the carbon–carbon contact points (Fig. 5). The presence of the Al–Si liquid phase at the C–C contact points allows soldering the carbon reinforcement in this zone and therefore to consolidate the carbon rigid network observed by x-ray tomography (Fig. 4). The formation of this carbon rigid network, induced by the liquid phase, can explain the decrease of the in-plane CTE of Al/(GF + CF) composite materials. The fact that the solid–liquid phase sintering generates a decrease of the in-plane CTE and an increase of the through-plane CTE (in average), compared to the PM route shows that the physical properties of the Al based composites in two direction are linked. This behavior is in accordance with the Firkowska formulation (Eq. 1). Indeed, the reduction of the in-plane CTE of Al/50 vol%GF composites with the solid–liquid phase sintering (from $21.8 \times 10^{-6}/K$ to $19 \times 10^{-6}/K$) induces a decrease of $\Delta\alpha_x$ (Eq. 2) and in-plane strain $\epsilon_{11} = \epsilon_{22}$. Then, the through-plane CTE of GF embedded in the matrix (α_{33} Eq. 1) will increase. This explains, therefore, the increase of the through-plane CTE of Al/GF composites with the solid–liquid phase sintering (from $-10.5 \times 10^{-6}/K$ to $-4.1 \times 10^{-6}/K$). With the addition of small amount of CF, the CTE value of (Al + Al–Si)/C composite fabricated by solid–liquid phase sintering can be controlled in order to obtain a CTE compatible to the ceramic domain ($2 \times 10^{-6}/K$ to $8 \times 10^{-6}/K$) in the in-plane direction or through-plane direction (Fig. 9a, d) without affecting significantly the in-plane TC of the composite materials (Fig. 7c).

3.7 Specific Thermal Conductivity of Al/(GF + CF) Composite Materials

Figure 11 shows the specific TC of Metal/C (with a reinforcement content close to 50 vol%) composites materials in function of CTE reported in the literature. Thanks to the low density of Al/50 vol%C (2.44 g/cm^3) and a high TC (411 W/m K), our MMC shows a high specific TC even higher than Cu/GF composite materials. Moreover Al/(GF + CF) shows a low CTE which make these composite materials compatible with electronic applications. In the ceramic domain, only Mg–Ca/GF composite shows a higher specific TC than our work thanks to the lightweight of the matrix.

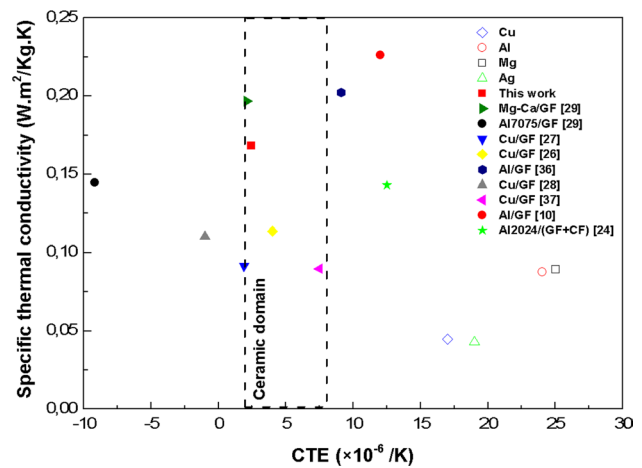


Fig. 11 Specific TC of $(Al_{90 \text{ vol}\%} + Al-Si_{10 \text{ vol}\%})/(GF + CF)$ (red square) compared to the Metal/C composite materials reported in the literature

4 Conclusion

The addition of 50 vol% of GF into the Al matrix improves remarkably the in-plane TC (400 W/m K). However, these materials show a through-plane CTE ($-10.5 \times 10^{-6}/K$) and in-plane CTE ($21.8 \times 10^{-6}/K$) incompatible with ceramic domain. Carbon fibers were added to Al/GF composite in order to increase the through-plane CTE and to decrease the in-plane CTE of Al/GF composite materials. It has been shown that by addition of (40 vol%GF + 10 vol%CF) to the Al matrix, induces a decrease of the in-plane CTE to $9.2 \times 10^{-6}/K$ which is significantly lower than an Al/10 vol%CF and Al/40 vol%GF composite materials ($18.9 \times 10^{-6}/K$ and $22.9 \times 10^{-6}/K$, respectively). The GF, in addition to increase the TC of the matrix, allows to decrease the mechanical percolation threshold of carbon fibers and then, provide the formation of a continuous and rigid (GF + CF) network that enhance the decrease of in-plane CTE.

In the through-plane direction, it has been shown that Al/(40 vol%GF + 10 vol%CF) composite exhibits a CTE of $17.6 \times 10^{-6}/K$ which is significantly higher than an Al/40%GF ($-6.4 \times 10^{-6}/K$) composite and lower than Al/10 vol%CF ($33 \times 10^{-6}/K$) composite. Recognizing that CF allows to increase the through-plane CTE, the GF/CF ratio was optimized for a total reinforcement of 50 vol% in order to control the value of the CTE without decrease significantly the in-plane TC of the composite materials.

Solid–liquid phase sintering was used to fabricate Al/C composites. The amount of liquid phase alloy was optimized for a carbon content of 50 vol%. The addition of 10 vol% of Al-12 wt%Si alloy to the matrix of Al/C composite materials induces:

- The increase of the relative densification of composite materials for reinforcement content of 50 vol%.
- The increase of the in-plane TC of Al/GF composite from 400 to 428 W/m K.
- The decrease of the in-plane CTE and the increase of through-plane CTE of Al/C composites materials.
- The presence of liquid phase in the carbon–carbon contact points leads to the formation of a solid CF + GF network.

Finally, two sets of (Al_{90 vol%} + Al–Si_{10 vol%})/50% Carbone composite materials have been developed and optimized:

- High in-plane TC (363 W/m K) and low in-plane CTE ($6.3 \times 10^{-6}/\text{K}$)
- High in-plane TC (411 W/m K) and low through-plane CTE ($2.4 \times 10^{-6}/\text{K}$)

Therefore, with their remarkable specific TC (0.168 W m²/Kg K), the composite materials developed in this study are applicable as a lightweight heat sink in micro-electronic industries.

Acknowledgement The authors thank the University of Bordeaux (2015-FD-24) for financial support.

References

1. C. Zweben, *JOM* **50**(6), 47–51 (1998)
2. C. Zweben: *Annual IEEE Semiconductor Thermal Measurement and Management Symposium*, pp. 168–174 (2005)
3. E. Rohatgi, K. Pradeep, *Def. Sci. J.* **43**(4), 323–349 (1993)
4. S. Mallik, N. Ekere, C. Best, R. Bhatti, *Appl. Therm. Eng.* **31**(2–3), 355–362 (2011)
5. K. Yoshida, H. Morigami, *Microelectron. Reliab.* **44**(2), 303–308 (2004)
6. P.W. Ruch, O. Beffort, S. Kleiner, L. Weber, P.J. Uggowitzer, *Compos. Sci. Technol.* **66**(15), 2677–2685 (2006)
7. O. Beffort, F.A. Khalid, L. Weber, P. Ruch, U.E. Klotz, S. Meier, S. Kleiner, *Diam. Relat. Mater.* **15**(9), 1250–1260 (2006)
8. H. Kurita, E. Feuillet, T. Guillemet, J.-M. Heintz, A. Kawasaki, J.-F. Silvain, *Acta Metall. Sin.* **27**(4), 714–722 (2014)
9. H.O. Pierson, *Handbook of Carbon, Graphite, Diamond and Fullerenes*, Noyes Publications Park Ridge (New Jersey, USA), 194–195 (1993)
10. J.K. Chen, I.S. Huang, *Compos. B Eng.* **44**(1), 698–703 (2013)
11. M. Murakami, N. Nishiki, K. Nakamura, J. Ehara, H. Okada, T. Kouzaki, K. Watanabe, S. Yoshimura, *Carbon* **30**(2), 255–262 (1992)
12. P.G. Klemens, D.F. Pedraza, *Carbon* **32**(4), 735–741 (1994)
13. Q. Fu, J. Yang, Y. Chen, D. Li, D. Xu, *Appl. Phys. Lett.* **106**(3), art. no. 031905 (2015)
14. Y. Huang, Y. Su, S. Li, Q. Ouyang, G. Zhang, L. Zhang, D. Zhang, *Compos. B Eng.* **107**, 43–50 (2016)
15. L. Weber, R. Tavangar, *Scripta Mater.* **57**(11), 988–991 (2007)
16. C. Azina, J. Roger, A. Joulain, V. Mauchamp, B. Mortaigne, Y.F. Lu, J.-F. Silvain, *J. Alloy. Compd.* **738**, 292–300 (2018)
17. J.M. Molina, E. Louis, *Mater. Charact.* **109**, 107–115 (2015)
18. C. Zhou, W. Huang, Z. Chen, G. Ji, M.L. Wang, D. Chen, H.W. Wang, *Compos. B Eng.* **70**, 256–262 (2015)
19. N. Chamroune, D. Mereib, F. Delange, N. Caillaud, Y. Lu, J.-L. Grosseau-Poussard, J.-F. Silvain, *J. Mater. Sci.* **53**(11), 8180–8192 (2018)
20. W. Li, Y. Liu, G. Wu, *Carbon* **95**, 545–551 (2015)
21. R. Prieto, J.M. Molina, J. Narciso, E. Louis, *Compos. A Appl. Sci. Manuf.* **42**(12), 1970–1977 (2011)
22. R. Prieto, J.M. Molina, J. Narciso, E. Louis, *Scripta Mater.* **59**(1), 11–14 (2008)
23. V. Oddone, J. Segl, M. Prakasam, M.T. Hartmann, J.-F. Silvain, C. Edtmaier, S. Reich, *J. Mater. Sci.* **53**(15), 10910–10919 (2018)
24. H. Kurita, T. Miyazaki, A. Kawasaki, Y.F. Lu, J.-F. Silvain, *Compos. A Appl. Sci. Manuf.* **73**, 125–131 (2015)
25. S. Ren, J. Chen, X. He, X. Qu, *Carbon* **127**, 412–423 (2018)
26. I. Firkowska, A. Boden, B. Boerner, S. Reich, *Nano Lett.* **15**(7), 4745–4751 (2015)
27. J. Chen, S. Ren, X. He, X. Qu, *Carbon* **121**, 25–34 (2017)
28. V. Oddone, B. Boerner, S. Reich, *Sci. Technol. Adv. Mater.* **18**(1), 180–186 (2017)
29. C.Y. Ho, R.W. Powell, P.E. Liley, *J. Phys. Chem. Ref. Data* **1**(2), 279–421 (1972)
30. V. Oddone, S. Reich, *Phys. Status Solidi. Rapid Res. Lett.* **11**(6), art. no. e201700090 (2017)
31. R.A. Schapery, *J. Compos. Mater.* **2**(3), 380–404 (1968)
32. G. Korb, J. Korab, G. Groboth, *Compos. A Appl. Sci. Manuf.* **29**(12), 1563–1567 (1998)
33. A. Bosak, M. Krisch, M. Mohr, J. Maultzsch, C. Thomsen, *Phys. Rev. B* **75**(15), 153–408 (2007)
34. V. Favier, R. Dendievel, G. Canova, J.Y. Cavaille, P. Gilormini, *Acta Mater.* **45**(4), 1557–1565 (1997)
35. C. Zhou, G. Ji, Z. Chen, M. Wang, A. Addad, D. Schryvers, H. Wang, *Mater. Des.* **63**, 719–728 (2014)
36. Q. Liu, X.-B. He, S.B. Ren, C. Zhang, L. Ting-Ting, X.H. Qu, *J. Alloy. Compd.* **587**, 255–259 (2014)

Publisher's Note Springer Nature remains neutral with regard to jurisdictional claims in published maps and institutional affiliations.